

High-Precision Inversion of Buried Depth in Urban Underground Iron Pipelines Based on AM-PSO Algorithm for Magnetic Anomaly

Pan Wu¹ and Zhiyong Guo^{2, *}

Abstract—Buried iron pipeline is an important part of urban infrastructure. In order to accurately obtain the location information of buried iron pipeline, here, we establish a forward model of magnetic anomaly in buried iron pipeline based on magnetic dipole reconstruction (MDR) method that determines four inversion parameters and two inversion objective functions. The vertical magnetic field data with different proportion noises are taken as observation values respectively to invert the parameters of underground pipeline and its location (buried depth) by using the AM-PSO (adaptive mutation particle swarm optimization) inversion algorithm. The errors of inversion and observation of vertical magnetic field are compared by substituting the inversion parameters into forward formulas. The results show that the AM-PSO inversion algorithm can accurately invert the pipeline depth, and the inversion error of the pipeline depth is less than 5%, which is acceptable in practical engineering. The inversion of the vertical magnetic field can basically coincide with the observed vertical magnetic field of the original model. At the same time, it is verified that the AM-PSO inversion algorithm is insensitive to magnetic anomaly noise data. In this study, the effectiveness of AM-PSO inversion algorithm method for pipeline depth inversion is analyzed, and an effective optimization inversion method is provided for underground iron pipeline depth inversion.

1. INTRODUCTION

Unscientific nature of history, geography, man-made and pipeline management often lead to errors, omissions, and deviations in the distribution of underground pipeline, which often cause the underground iron pipeline to be broken or leaked in the process of urban infrastructure construction and pipeline encrypt laying [1, 2]. Therefore, it is an urgent problem to be solved in the development and management of modern pipeline construction which improves detection, distribution, and management information of underground pipeline.

Iron pipeline accounts for the majority of existing pipelines, which generates a magnetizing field under the magnetization of the geomagnetic field. Then the superposition of magnetizing field on original magnetic field affects the distribution of original magnetic field and forms magnetic anomaly. By analyzing the distribution characteristics of magnetic anomalies on the detection plane and using the method of magnetic anomaly data processing and inversion, we can judge the existence of underground pipeline and determine the horizontal position and burial depth of pipeline. So far, many scholars have done research on inversion of magnetic anomaly. McGrath and Hood [3] proposed a least squares multi-model magnetic anomaly inversion method, which was used to invert the magnetic anomaly of different models such as finite-length thick levees, vertical prism, and parallelepiped, and obtained the geometric information of the model appearance. Based on the joint derivation of analytical signal and Euler deconvolution method (Analytic signal-Euler's equation), Salem and Ravat [4] proposed a new method

Received 7 November 2019, Accepted 12 January 2020, Scheduled 18 February 2020

* Corresponding author: Zhiyong Guo (zhy-guo@hotmail.com).

¹ College of Mechanical and Electrical Engineering, Southwest Petroleum University, Chengdu 610500, China. ² Department of Biomedical Engineering, Southern University of Science and Technology, Shenzhen 518055, China.

of automatic interpretation of magnetic data. By using this method, the position and approximate geometry of magnetic source can be obtained. Salem and Smith [5] proposed a simple method for estimating the location and model type of two-dimensional magnetic source using normalized first-order local wave number. Abdelrahman and Essa [6] obtained the second-order horizontal derivative of magnetic anomaly data from magnetic data by using continuous window length filter and determined the depth and shape of buried magnetic anomaly structure. Tlas and Asfahani [7] proposed a simplex algorithm for optimal estimation of magnetic parameters of simple geometric structures, which is based on deconvolution technique and linear programming with simplex algorithm to estimate the model parameters, such as the depth from the geomagnetic anomaly profile to the top or center, effective magnetization angle, and amplitude coefficient. This method has certain anti-noise ability. Gokturkler and Balkaya [8] adopted genetic algorithm (GA) and simulated annealing algorithm (SA) to invert the magnetic anomalies generated by some of simple geometric polarization body, and the solutions are very close to the real model parameters obtained. Biswas proposed a very fast simulated annealing (VFSA) global optimization algorithm to explain gravity and magnetic anomalies in thin-layer structures [9]. The optimization results showed that the method could uniquely determine all model parameters in the case of determined magnetic anomalies, and the calculation time of the whole process is very short. Ekinici [10] used the numerical second-order, third-order and fourth-order horizontal derivatives calculated from the observed magnetic anomalies to estimate the depth of an isolated dike-like magnet source body. This method does not require prior information and is in line with the real results. So far, there are few inversion studies on pipeline magnetic anomaly. Generally, the magnetic anomaly component calculated by the obtained model parameters can accurately match the magnetic anomaly observation component when the total magnetic anomaly is used as the observation value for inversion, but it is necessary to calibrate and record the orientation of magnetic field sensor in real time for actual engineering applications, and the operation is complicated and prone to human interference. Therefore, we consider using one of the three components of the total magnetic anomaly to invert the pipeline parameters. Among them, the X component and Y component need multi-sensor geographical orientation alignment in the process of detection, which results in low accuracy in engineering. On the contrary, the Z component (vertical magnetic field) only needs to be determined by just one gravity sensor in vertical direction. At the same time, according to the distribution of geomagnetic inclination and geomagnetic declination, we can know that the component of geomagnetic field in Z -axis (vertical downward) is the largest and has the strongest magnetization effect on the pipeline. Therefore, the vertical magnetic field as the observation value has higher measurement accuracy. The geomagnetic field has the largest component on the Z -axis (vertically downward), thus the strongest magnetization effect on the pipeline. Therefore, the vertical magnetic field is used as an observation value to have a high measurement accuracy.

Here, based on the principle of magnetic dipole reconstruction (MDR), we first establish the forward model to calculate the magnetic field of pipeline. Two objective functions are proposed from the vertical magnetic field for the AM-PSO inversion algorithm to invert the four parameters of pipeline, i.e., diameter, thickness, burial depth, and magnetic susceptibility many times, and the actual final inversion parameter determined as the buried depth of pipeline. In addition, the error of depth inversion and the restoration of vertical magnetic field curve are also analyzed when the observed vertical magnetic field data contain different sizes of noise. The results of inversion prove the accuracy and effectiveness of pipeline depth using (AM-PSO) inversion algorithm.

2. FORWARD MODEL AND METHOD

2.1. Magnetic Anomaly Forward Method and Parameters

Accurate magnetic anomaly forward calculation of underground iron pipeline is the prerequisite for accurate inversion. We establish a coordinate system as shown in Fig. 1. The X -axis is geographic north, Y -axis geographical east, and Z -axis perpendicular to the XOY plane vertically downward. B_e is the total geomagnetic field strength, D the magnetic declination, I_c the magnetic inclination, and the other components of the geomagnetic field can be calculated by these three independent components. The iron pipeline generates an anomalous field under the magnetization of geomagnetic field, which can be detected on the detection plane after being superimposed with the geomagnetic field. The magnetic

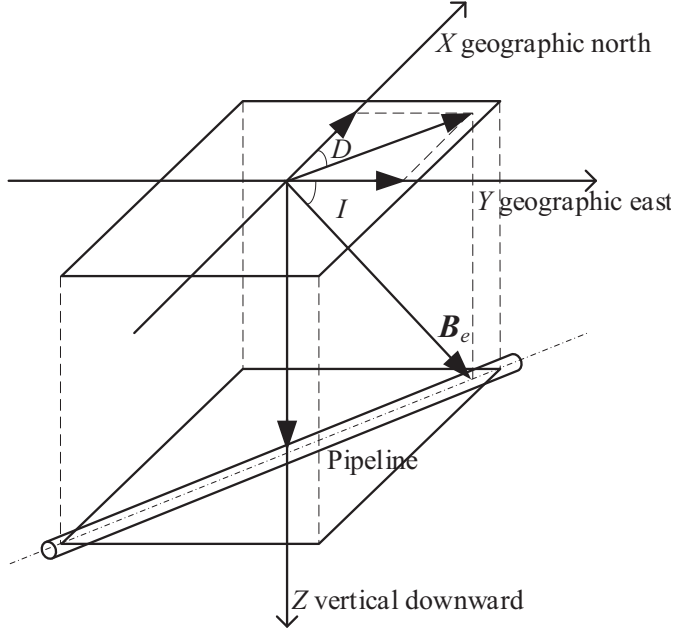


Figure 1. Geomagnetic coordinate system for pipeline detection.

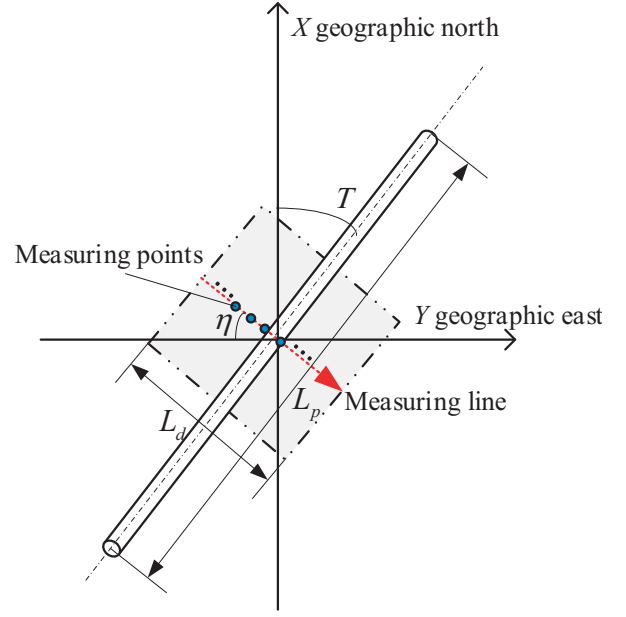


Figure 2. Top view of magnetic anomaly detection area of pipeline.

anomaly inversion is to obtain the characteristic information of underground pipeline by analyzing the anomalous field detected. Fig. 2 is a top view of the detection plane, and Fig. 3 is a cross-sectional view of the pipeline. The detection plane is parallel to the horizontal ground; the measuring line is perpendicular to the axis of the pipeline; and the midpoint of the measuring line is directly above the axis of the pipeline. The height of the measuring line is h_2 ; the length is L_d ; the azimuth is η ; setting the angle between the pipeline and the X -axis is θ ; the length of the pipeline is L_p ; the outer diameter of pipeline is ϕ ; the thickness is δ ; the buried depth is h_1 ; and the magnetic susceptibility of the pipeline is χ_m . Due to the large geometry size of the pipeline, it cannot be regarded as a magnetic dipole to directly calculate the magnetic field strength at the detection plane. The previous research results by Guo et al. show that the magnetic field of the underground pipeline in the detection plane can be accurately calculated by using the MDR method [11]. Therefore, based on this principle, the pipeline is divided into a large number of tiny volume elements E_i (as shown in Fig. 4). For each tiny volume element, its magnetic field values at each measuring point on a measuring line can be solved by using the magnetic dipole formula. Then the magnetic field values of all the tiny volume elements at the same measuring point P_j are vector superimposed, and the same is true for other measuring points. Suppose that the total number of tiny volume elements obtained from pipeline is I and that the total number of measuring points on one measuring line is J . The magnetic anomaly vector composed of the total magnetic anomaly of all the measuring points on the measuring line is recorded as $\mathbf{B}_d = [\mathbf{B}_1, \mathbf{B}_2, \dots, \mathbf{B}_j, \dots, \mathbf{B}_J]$, where \mathbf{B}_j is the superposition of the geomagnetic field and measuring line magnetic anomaly which is equal to the sum of magnetic field vectors of all the pipeline tiny volume elements $E_i(E_{ix}, E_{iy}, E_{iz})$ at the measuring point $P_j(P_{jx}, P_{jy}, P_{jz})$. The calculation formulas are shown as Eqs. (1)–(4) [11–13].

$$\mathbf{B}_j = \frac{\mu_0}{4\pi} \sum_{i=1}^I \left(\frac{3(\mathbf{m}_{ij} \cdot \mathbf{r}_{ij}) \mathbf{r}_{ij}}{r_{ij}^5} - \frac{\mathbf{m}_{ij}}{r_{ij}^3} \right) + \mathbf{B}_e \tag{1}$$

$$r_{ij} = \sqrt{(P_{jx} - E_{ix})^2 + (P_{jy} - E_{iy})^2 + (P_{jz} - E_{iz})^2} \tag{2}$$

$$\mathbf{m}_{ij} = V \cdot \chi_m \cdot \mathbf{H}_{ij} \tag{3}$$

$$\mathbf{H}_{ij} = \frac{\mathbf{B}_e}{\mu_0} \tag{4}$$

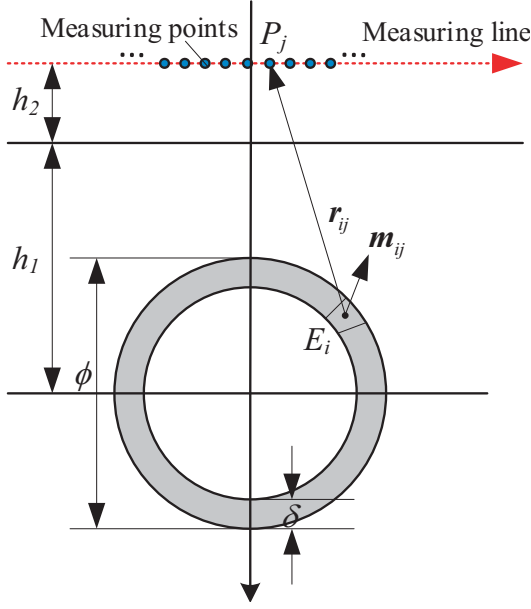


Figure 3. Vertical cross-sectional view of the pipeline.

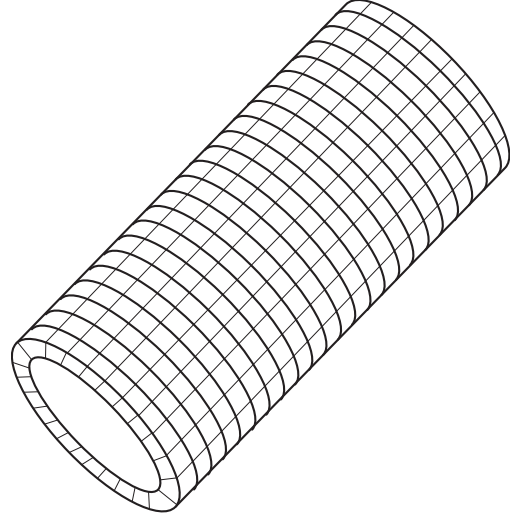


Figure 4. Cell segmentation model.

In Equation (1), $\mu_0 = 4\pi \times 10^{-7} (\text{H} \times \text{m}^{-1})$ is the vacuum permeability. \mathbf{r}_{ij} is the position vector from the tiny volume element E_i to the measuring point P_j , and r_{ij} is its modulus, which can be calculated by Formula (2). \mathbf{m}_{ij} is the magnetic moment of the tiny volume element E_i at the measuring point P_j obtained by Equation (3). V is the volume of the tiny volume element. χ_m is the magnetic susceptibility of the pipeline material. \mathbf{H}_{ij} is the strength of the external magnetic field at the location of E_i , which can be calculated by Equation (4).

From the derivation process of the above magnetic anomaly calculation formula, it can be known that the distribution characteristics of pipeline magnetic anomalies are determined by the position parameters of pipelines, geometric characteristics parameters of pipelines, measuring line parameters and geomagnetic field parameters. Among them, the geometric characteristics of pipeline are characterized by three parameters: pipeline length L_p , pipeline outer diameter ϕ , and pipeline thickness δ , which determine the size of dividing unit V . The position information of the pipeline is characterized by two parameters: pipeline azimuth θ ($0 \leq \theta \leq \pi$) and pipeline burial depth h_1 , which, together with the measuring line parameters, determine the position vector \mathbf{r}_{ij} . The background geomagnetic field is characterized by three independent geomagnetic elements: total strength B_e , magnetic inclination I_c , and magnetic declination D , from which external magnetic field strength \mathbf{H}_{ij} at the location of the pipeline can be derived. When studying the magnetization field of pipeline, only the magnetic susceptibility of pipeline should be considered. Therefore, the total magnetic anomaly vector \mathbf{B}_d on the measuring line can be expressed as a function of 12 parameters:

$$\mathbf{B}_d = f(L_p, \phi, \delta, \theta, h_1, B_e, I_c, D, \chi_m, h_2, L_d, \eta) \quad (5)$$

From the function in Eq. (5), the relationship between the magnetic anomaly forward parameters of the iron pipeline and the total magnetic anomaly is established. The vertical magnetic field only needs to take the vertical downward component of \mathbf{B}_d , which is recorded as \mathbf{B}_z .

2.2. Theoretical Inversion Parameters

The inversion of magnetic anomalies in iron pipeline is to find an optimal model to minimize the errors between the calculated magnetic anomalies and the measured magnetic anomalies [14]. Suppose that the observed total magnetic anomaly vector of the measuring line is \mathbf{B}^{obs} , and the total magnetic anomaly vector of the measuring line obtained by theoretical numerical calculation is \mathbf{B}^{sim} . The inversion process of magnetic anomaly is to find a set of parameters to make \mathbf{B}^{sim} as close as possible to \mathbf{B}^{obs} .

During the magnetic anomaly detection process, the length and height of the measuring line are known, i.e., h_2 and L_d are known quantities in the three parameters of Equation (5). Since the direction of the measuring line is perpendicular to the direction of the underground iron pipeline, the measuring line azimuth angle η can be determined by the pipeline azimuth angle θ which is determined by the line connecting the peaks of the vertical magnetic field [15]. The background geomagnetic field can be regarded as a constant magnetic field in a small area and a short time [16]. The geomagnetic field which is perpendicular to the direction of the pipeline and is not affected by other magnetic anomalies can be regarded as a reference geomagnetic field [17, 18]. Therefore, the background geomagnetic field strength B_e , magnetic inclination I_c , and magnetic declination D can be measured beforehand. The length of the horizontal single pipeline actually laid is generally greater than 20 m, so the magnetic anomaly detected in a small area near the midpoint of the pipeline is in two-dimensional body magnetic anomaly distribution, and the further increase of the pipeline length does not contribute much to the magnetic anomaly of the measuring line. Therefore, in the process of simulation, the magnetic anomaly caused by 20 m long pipeline can be used to replace the magnetic anomaly caused by second-degree body pipeline, i.e., $L_p = 20$ m. Finally, only 4 of the 12 model parameters of the function in Eq. (5) are unknown, and the function in Eq. (5) can be simplified as:

$$\mathbf{B}_d = g(\phi, \delta, h_1, \chi_m) \quad (6)$$

3. OBJECTIVE FUNCTION AND AM-PSO

3.1. Inversion Objective Function

Actual magnetic anomaly observation data \mathbf{B}^{obs} is derived from the detection of pipeline magnetic anomaly, but here we use synthetic data as magnetic anomaly observation data in the process of theoretical research. The real pipeline magnetic anomaly data obtained by the forward formula (1) is recorded as \mathbf{B}^{true} , and the magnetic anomaly noise is recorded as \mathbf{B}^{noise} , then \mathbf{B}^{obs} can be expressed by Equation (7):

$$\mathbf{B}^{obs} = \mathbf{B}^{true} + \mathbf{B}^{noise} \quad (7)$$

During the inversion process, the four parameters $(\phi, \delta, h_1, \chi_m)$ in the function of Eq. (6) are continually searched by the AM-PSO inversion algorithm, and the inversion vertical magnetic field is obtained by substituting the four parameters into Equation (1), which is recorded as \mathbf{B}^{sim} . The purpose of inversion is to make the difference between \mathbf{B}^{sim} and \mathbf{B}^{obs} meet the requirement of fitness threshold. The validity and accuracy of the AM-PSO inversion algorithm are studied by using magnetic anomaly values with noise or not as observation data.

When there is no magnetic abnormal noise, the maximum value of the difference between \mathbf{B}^{sim} and \mathbf{B}^{obs} can be used as the objective function value to measure the magnetic anomaly. In this case, the objective function can be expressed as the infinite norm of the two magnetic anomaly vectors [19]:

$$\phi = \left\| \mathbf{B}^{obs} - \mathbf{B}^{sim} \right\|_{\infty} \quad (8)$$

When the observed value \mathbf{B}^{obs} of magnetic anomaly contains a certain amount of noise, in order to make \mathbf{B}^{sim} fit the \mathbf{B}^{obs} curve as much as possible, the standard deviation of the error between \mathbf{B}^{sim} and \mathbf{B}^{obs} must be minimized. In this case, the objective function is expressed as the 2-norm of the two magnetic anomaly vectors [19, 20]:

$$\phi = \left\| \mathbf{B}^{obs} - \mathbf{B}^{sim} \right\|_2 \quad (9)$$

3.2. AM-PSO Algorithm for Vertical Magnetic Field

The particle swarm optimization (PSO) algorithm is a global intelligent optimization method to simulate the foraging behavior of birds and fish. The PSO algorithm was first proposed by Eberhart and Kennedy in 1995. The algorithm does not need to set the search starting point and can search directly within the target value range [21, 22]. Later, after years of development and research, the algorithm has been improved in many aspects. Merchaoui et al. [23] introduced the particle adaptive mutation mechanism

to effectively avoid the premature convergence problem of particle swarm optimization algorithm and improved the accuracy of algorithm search. The basic particle swarm particle position calculation formula and velocity update formula are as shown in Equations (10) and (11) [21]:

$$\mathbf{v}_s^{p+1} = w\mathbf{v}_s^p + c_1\text{rand}(1) (\mathbf{X}_{sbest}^p - \mathbf{X}_s^p) + c_2\text{rand}(1) (\mathbf{X}_{gbest}^p - \mathbf{X}_s^p) \quad (10)$$

$$\mathbf{X}_s^{p+1} = \mathbf{X}_s^p + c_3\mathbf{v}_s^{p+1} \quad (11)$$

The calculation method of the d th variable mutation method of the s th particle of the p th generation is as follows [24, 25]:

$$\mathbf{X}_{sd}^{p+1} = \begin{cases} \mathbf{X}_{d\min} + (\mathbf{X}_{d\max} - \mathbf{X}_{d\min})\text{rand}(1), & 1 - \text{rand}(1) > c_4, (d = \lceil 2\text{rand}(1) \rceil) \\ \mathbf{X}_{sd}^{p+1}, & \text{others} \end{cases} \quad (12)$$

In Equations (10)–(12), \mathbf{v}_s^p is the search speed of the s th particle of p th generation, $p=1, 2, \dots, P$, $s=1, 2, \dots, S$; \mathbf{v}_s^{p+1} is the search speed of the s th particle of $(p+1)$ th; c_1 and c_2 are learning factors; c_3 and c_4 are a constraint factors; w is the inertia weight; $\text{rand}(1)$ is a random value in the range $[0, 1]$, and the result is different each time the function is run; \mathbf{X}_s^p is the position the s th particle of p th generation; \mathbf{X}_{sbest}^p is the individual optimal value of the s th generation and previous generations; \mathbf{X}_{gbest}^p is the global optimal value of the p th generation and previous generations; \mathbf{X}_{sd}^{p+1} is the d th dimensional variable of the s th particle in the $(p+1)$ th generation; $\mathbf{X}_{d\max}$ and $\mathbf{X}_{d\min}$ are the maximum and minimum values of the D -dimensional variable within its range of variation, respectively.

The algorithm flow of using the adaptive mutation particle swarm optimization algorithm to invert the buried depth of the pipeline is shown in Fig. 5. The specific algorithm steps are as follows:

- 1) Set algorithm parameters: particle swarm size $S = 30$, evolution algebra $P = 40$, learning factors $c_1 = c_2 = 2.05$, inertia weight $w = 0.8$, constraint factor $c_3 = 0.8$, mutation probability $c_4 = 0.2$, pipeline depth h_1 , search range $[0.2, 6]$ (m), magnetic susceptibility χ_m search range $[0.001, 100]$ (SI), and define the initial position of the particle as $\mathbf{X} = [\phi, \delta, h_1, \chi_m]$ and speed as $\mathbf{V} = \mathbf{X} * 0.1$.
- 2) Initialization of the optimal fitness value: Equation (8) or (9) is used to calculate the fitness value φ_s^1 of each particle of the first generation. Set φ_s^1 as the optimal fitness value of a single particle \mathbf{X}_{sbest}^1 . Comparing the fitness values of all particles, the optimal fitness value is selected as the global optimal fitness value \mathbf{X}_{gbest}^1 of the first-generation particle group.
- 3) Position and speed update: update the particle velocity and the position of the particle in the search space using Equations (10) and (11), and introduce the particle mutation to prevent the algorithm from falling into local optimum according to Equation (12).
- 4) Recalculate the fitness value of each particle. If the obtained local particle optimal fitness value or global optimal fitness value is better than the corresponding value of the previous generation particle, update the corresponding single particle local optimal fitness value or global optimal fitness value.
- 5) If the global optimal particle objective function value is less than the threshold or reaches the maximum evolution algebra, the final solution will be output and terminated. Otherwise, step 3) will be returned and recalculated.

3.3. Actual Inversion Parameters

Table 1 contains model parameters for generating theoretical observation of the vertical magnetic field. When the parameter optimization inversion is performed, the non-inversion parameters are the same as the parameters in Table 1. If the generated vertical magnetic field is directly taken as observation data \mathbf{B}^{obs} , since the observation data are theoretically generated and without noise, a perfect particle $\mathbf{X} = (\phi, \delta, h_1, \chi_m)$ can be found theoretically in accordance with the corresponding parameters in Table 1. The magnetic anomaly inversion is performed according to the model parameters in Table 1. The inversion results are shown in Table 2, which indicate that only the pipeline buried depth is close to the original model's depth, and the stability of the inversion of buried depth is very good for many times. The other three inversion parameters are quite different from the original model parameters, and

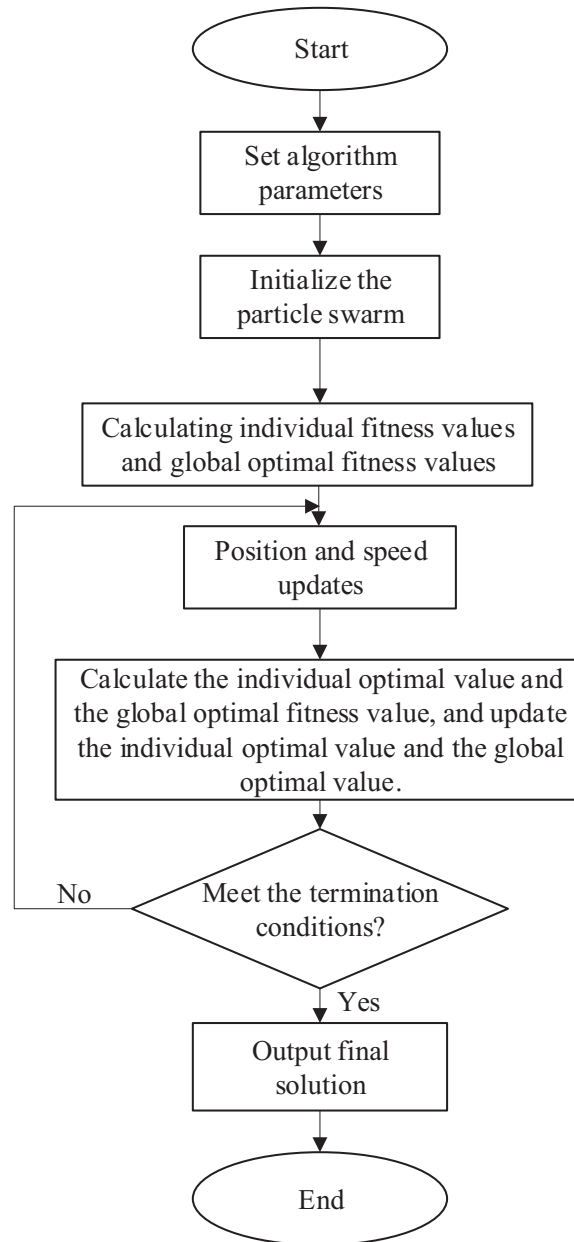


Figure 5. The flow chart of optimizing inversion of vertical magnetic field utilizing AM-PSO.

the inversion results have little reference value. Therefore, this paper only takes the inverted pipeline buried depth as the research object, and pipeline buried depth is also the most concerned parameter of pipeline inversion detection.

Table 1. Forward parameter settings of generating magnetic anomaly vertical component.

Parameters	Pipeline parameters						Geomagnetic parameters			Measuring line path		
	ϕ (cm)	δ (mm)	L_p (m)	χ_m (SI)	θ (°)	h_1 (m)	B_e (nT)	I_c (°)	D (°)	h_2 (cm)	L_d (m)	η (°)
Values	60	10	30	30	60	2	54583.6	59.061	-6.629	10	14	90

Table 2. Inversion results of utilizing AM-PSO.

Parameters	Serial number	ϕ (cm)	δ (mm)	χ_m (SI)	h_l (cm)
Inversion parameters	1	21.21	13.96	63.98	200.02
	2	41.66	11.26	38.64	199.58
	3	69.50	14.99	17.37	200.01
	4	71.69	9.38	26.49	198.94
	5	99.99	8.57	20.82	199.79
	6	39.87	6.74	67.15	200.30
	7	41.62	10.55	41.37	199.97
	8	94.27	10.65	17.85	200.05
	9	71.51	13.46	18.75	200.01
	10	166.90	3.52	30.56	201.59
Original parameters		60	10	30	200

4. CASE ANALYSIS

4.1. Depth Inversion with Noise or Not

From 0.5 m to 5 m, a pipeline depth value is taken every 0.5 m, and a total of 10 inversions are performed, denoting the number of inversions as ξ . Other parameters are shown in Table 1. The noise-free observation magnetic vertical field is obtained by superimposing the vertical component of the geomagnetic field with the vertical magnetic anomaly calculated by Equation (1) based on previous model parameters. Then the noise-free observation magnetic field is combined with the objective function for noise-free inversion. The noise-containing observation vertical magnetic field is obtained by superposition of the noise-free observation magnetic vertical field and random noise with a peak value of 5 nT caused by geomagnetic fluctuation, instrument circuit, sensor accuracy, and combined with the objective function in Eq. (9), the depth inversion calculation of noisy pipeline is carried out. The result is shown in Fig. 6. It can be seen from Fig. 6 that the depths obtained by performing 10 inversions are basically consistent with the original buried depth of pipeline, and the error of noise-containing inversion

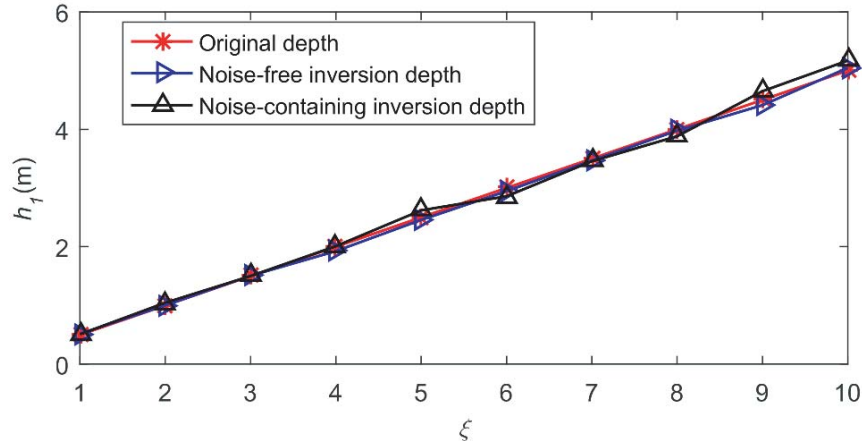


Figure 6. Comparison of noise-free inversion depth, noise-containing inversion depth, and original depth.

is slightly larger than that of the noise-free inversion, but the difference between them is small. Fig. 7 shows the error comparison between noise-free inversion and noise-containing inversion for 10 times. It can be seen from Fig. 7 that the maximum relative error in the noise-free inversion occurs in the 5th inversion and its value is 4.78%. In addition, the average error of 10 inversions is 1.59%. The maximum relative error in the noise-containing inversion occurs in the 1st inversion and its value is 3.76%, and the average relative error of 10 inversions is 2.73%. Therefore, we could know that all the inversion errors of buried pipeline depth obtained by the AM-PSO algorithm are less than 5% in our research cases, which are acceptable in actual engineering [26]. At the same time, the comparison of inversion errors indicates that the use of AM-PSO algorithm for pipeline depth inversion has high accuracy and certain anti-noise ability. Take the buried depth of the pipeline as 1, 2, 3, 4, 5 m respectively to study the convergence of particle swarm optimization algorithm. It can be seen from Fig. 8 that the particle swarm optimization algorithm has achieved good inversion results under different buried depths, without any non-convergence phenomenon. The average number of evolutions for 5 inversions is 15.6 times (set the total number of evolutions to 40 times); the average time of inversion algorithm is 20.08 s; and the computer memory is 1712 MB. Therefore, compared with other inversion algorithms, particle swarm optimization algorithm has a greater advantage in pipeline inversion in terms of its inversion accuracy, speed, and consumption of computer hardware resources [27].

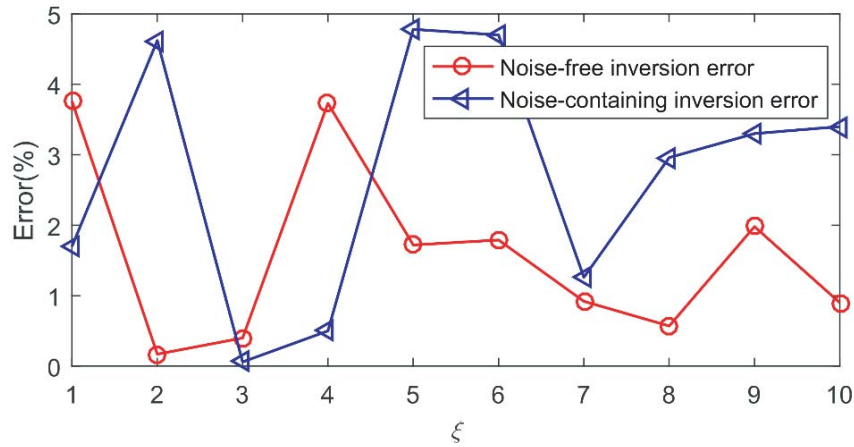


Figure 7. Error comparison between noise-free inversion and noise-containing inversion.

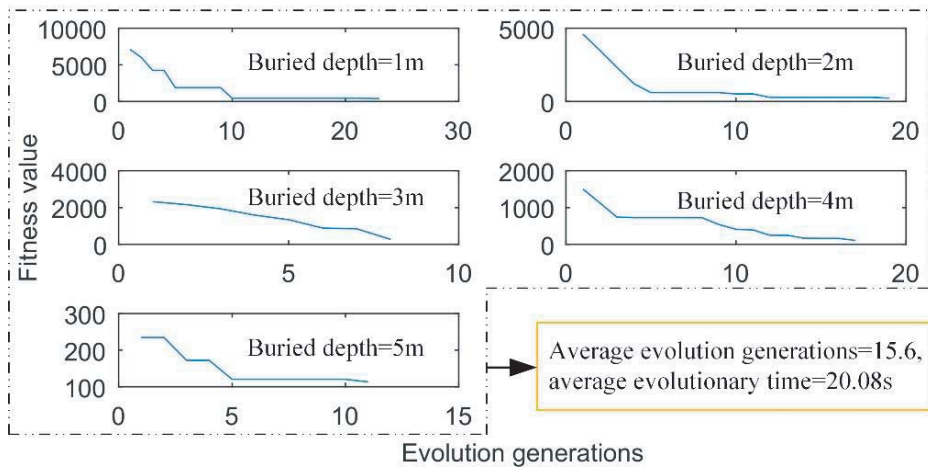


Figure 8. Convergence curves for multiple inversion depths.

4.2. Noise Sensitivity Test

The main sources of noise contained in the observation vertical magnetic anomalies are the measurement accuracy of the sensor, the voltage fluctuation of the detection circuit, and the fluctuation of the environmental magnetic field. From the previous analysis, it is found that the AM-PSO algorithm has certain anti-noise ability in pipeline depth inversion. Furthermore, in order to analyze the anti-noise ability of the AM-PSO algorithm, the calculated vertical magnetic fields with the buried depths of 1, 3, 5 m are randomly taken, and random noise signals with different peak-to-peak values are added. According to Biot · Savart's law, with the depth of the pipeline increasing, the strength of the magnetic field decreases rapidly with the cube depth. Therefore, different percentages of noise signals should be added according to different pipeline depths. Here, taking the maximum peak value of noise signal as ω (defined as the ratio of noise to magnetic field and denoted as ω) times of the maximum magnetic fluctuation, then superimpose the noise signal and calculated vertical magnetic field as the observed magnetic field. Calculated by Equation (1), the maximum magnetic field fluctuation on the detection plane is 898.42 nT when the buried depth of the pipeline is 1 m, and the maximum noise peak is shown in the last row of the first column of Table 3, which respectively accounts for 10%–90% of the observed magnetic field (step size is 10%). Similarly, when the original buried depth is 3 m or 5 m, the noise magnetic field is also taken according to the noise-to-magnetic ratio of 1 m. The maximum noise peak value is shown in Table 3.

Table 3. The influence of noise on inversion depth when utilizing AM-PSO.

Buried depth (m)	1	3	5
Maximum fluctuation value (nT)	898.42	121.12	43.39
Percentage of noise (%)	1 ~ 90	1 ~ 90	1 ~ 90
Maximum noise peak (nT)	89.84 ~ 808.58	12.11 ~ 109.01	4.39 ~ 39.05

Pipeline depth inversion is performed according to the noise-to-magnetic ratio in Table 3. The results are shown in Fig. 9. It can be seen from Figs. 9(a) and (b) that under the same pipeline original buried depth, with the increase of noise-to-magnetic ratio (10%–90%) gradually, the inversion depth changes little, which is basically consistent with the original buried depth of the pipeline. The relative errors in the 7th inversion at the original buried depths of 1 m, 3 m, and 5 m reach the maximum, which

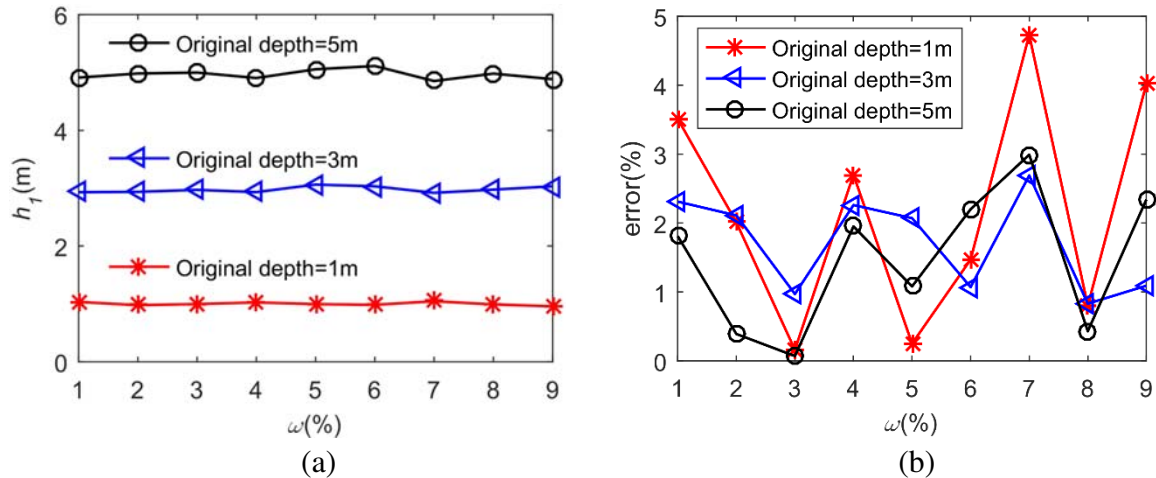


Figure 9. Influence of different noise-magnetic ratio on depth inversion under different burial depth and the relative error. (a) Influence of different noise-magnetic ratio on depth inversion under different burial depth; (b) Inversion errors of different noise-magnetic ratio under different buried depths.

are 2.76%, 2.98%, and 4.87%, respectively. The relative errors are still within the 5% range which is allowed by the project, and the corresponding noise-to-magnetic ratio is almost up to 70%, which indicate that the AM-PSO algorithm has strong anti-noise ability and can perform pipeline depth inversion under complex conditions. Fig. 9(b) shows that the relative errors of the different buried depths are basically consistent with the variation trend of the noise-to-magnetic ratio, and the relative errors of the different buried depths are relatively close when the noise-to-magnetic ratio is the same. Further calculation shows that the average relative error at 5 m depth is 1.47%, at 3 m depth is 1.71%, and at 1 m depth is 2.18%, which indicates that in a certain pipeline buried depth range under the same noise-to-magnetic ratio, the larger the buried depth is, the better the inversion effect is. It shows that the vertical magnetic field inversion method of AM-PAO is highly adaptable to weak magnetic environment. The average value obtained by multiple inversion can effectively improves the accuracy and inversion stability of buried depth.

4.3. Noisy Vertical Magnetic Field Inversion Recovery B_z

Randomly take the actual depth of the two pipelines, which may be 2 m and 3 m. The vertical magnetic field calculated by each original buried depth is added with 10%, 30%, 60% noise-to-magnetic ratio magnetic field. Combined with the inversion objective function in Eq. (9), the pipeline depth inversion is performed, and the results are shown in Fig. 10. Figs. 10(a) and (c) are the magnetic anomaly

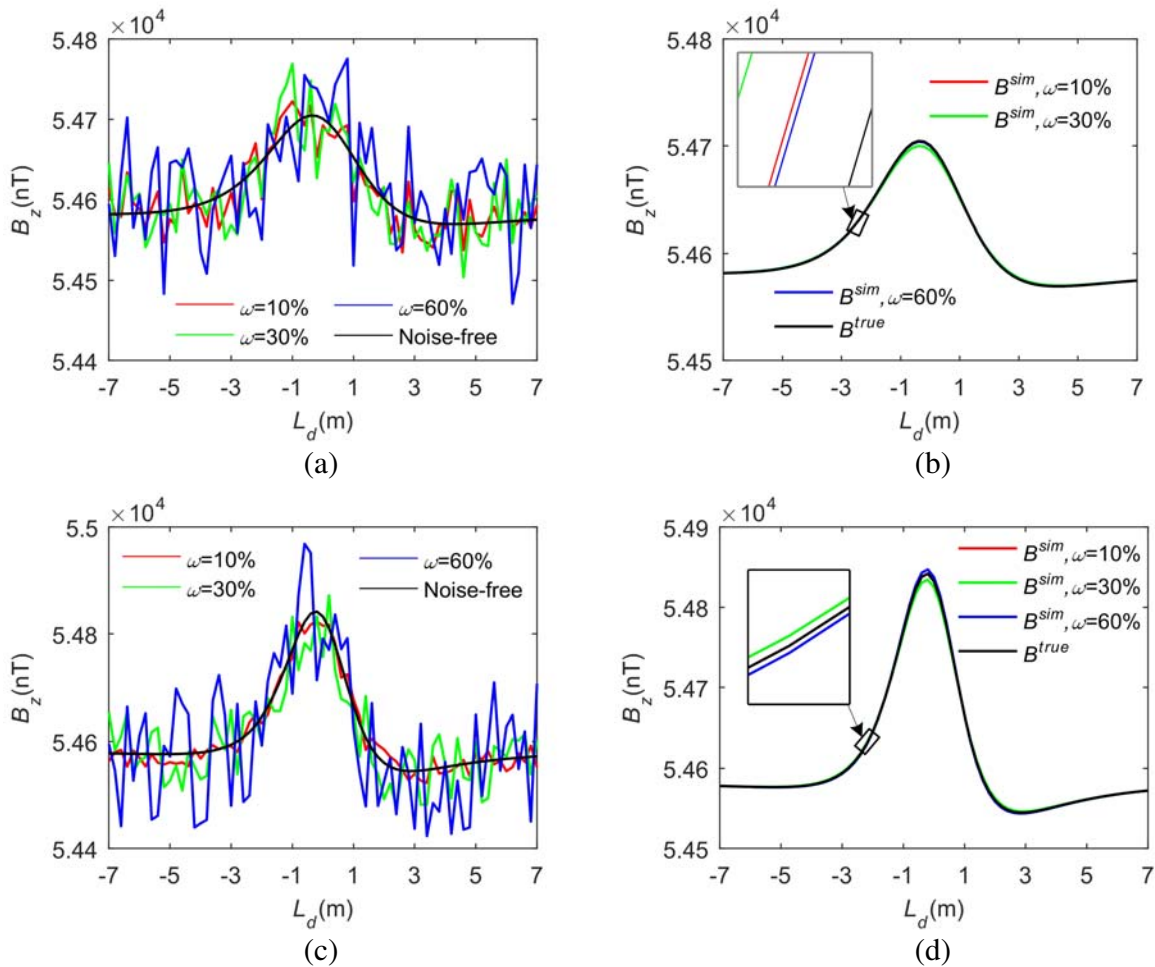


Figure 10. Vertical magnetic field with different noise-to-magnetic ratio and inversion to restore the original vertical observed magnetic field. (a), (c) Vertical magnetic field with different noise-to-magnetic ratio at original depth of 2 m and 3 m; (b), (d) Comparison of vertical magnetic field recovery with different noise-to-magnetic ratio.

fluctuation curves obtained on the measuring line under three kinds of noise-to-magnetic ratio and noise-free conditions when the buried depths of the pipeline are 2 m and 3 m, respectively. The inversion depths of the pipelines are 1.9599, 2.002, 2.0504, and 3.0081 m, 3.0623 m, 3.0174 m respectively under three conditions of noise-to-magnetic ratio. Figs. 10(b) and (d) show the fluctuation trend of true vertical magnetic field B^{true} and vertical magnetic field B^{sim} with different noise-to-magnetic ratio noisy signal under two buried depths. Enlarged view (shown in the box) shows that when the actual buried depth is 2 m, the degree of matching between the inversion vertical magnetic field B^{sim} and the true vertical magnetic field B^{true} is sorted as $\omega=60\% > \omega=10\% > \omega=30\%$. When the true buried depth is 3 m, the matching degree is ranked as $\omega=10\% > \omega=60\% > \omega=30\%$. Therefore, in a certain range, the high noise-to-magnetic ratio is not necessarily related to the inversion accuracy. The vertical magnetic field obtained by the AM-PSO algorithm can be highly consistent with the vertical magnetic field calculated by the original model parameters. The obtained model parameters can effectively recover the vertical magnetic anomaly, which proves the effectiveness of the inversion using the AM-POS algorithm.

5. CONCLUSION

Based on the magnetic dipole reconstruction (MDR) method, the forward model of magnetic anomaly in the vertical magnetic field of underground pipeline is established, and the calculation method of the vertical magnetic field of pipeline is derived. Firstly, taking the vertical magnetic field with different noise-magnetic ratios as the observation value, the adaptive mutation particle swarm optimization (AM-PSO) inversion algorithm is used to inverse the buried depth of pipeline. Then the relative errors of the inverted depth of the vertical magnetic field with different noise-to-magnetic ratios at multiple inversion depths are compared. Finally, the original vertical magnetic field is basically restored by using the inverted pipeline depth. The main conclusions are as follows:

- 1) Four inversion parameters and two inversion objective functions are determined based on the prior information or references.
- 2) The buried depth of the pipeline can be basically consistent with the original pipeline buried depth, and the average relative error of the buried depth of the pipeline is less than 5%, which are acceptable in actual engineering.
- 3) The depth of the inverted model parameters can basically coincide with the original burial depth, while the other three parameters have low coincidence. In addition, the inverted vertical magnetic field highly matches the original observed vertical magnetic field.
- 4) The adaptive mutation particle swarm optimization (AM-PSO) inversion algorithm is insensitive to noise and has strong anti-noise ability.

ACKNOWLEDGMENT

This work was supported in part by the National Natural Science Foundation of China under Grant 41374151.

REFERENCES

1. McConnell, T. J., B. Lo, A. Ryder-Turner, and J. A. Musser, "Enhanced 3D seismic surveys using a new airborne pipeline mapping system," *SEG Technical Program Expanded Abstracts*, 516–519, 1999.
2. Allred, B. J. and J. D. Redman, "Location of agricultural drainage pipes and assessment of agricultural drainage pipe conditions using ground penetrating radar," *Journal of Environmental and Engineering Geophysics*, Vol. 15, No. 3, 119–134, 2010.
3. McGrath, P. H. and P. J. Hood, "An automatic least-squares multimodel method for magnetic interpretation," *Geophysics*, Vol. 38, No. 2, 349–358, 1973.
4. Salem, A. and D. Ravat, "A combined analytic signal and Euler method (AN-EUL) for automatic interpretation of magnetic data," *Geophysics*, Vol. 68, No. 6, 1952–1961, 2003.

5. Salem, A. and R. Smith, "Depth and structural index from normalized local wavenumber of 2D magnetic anomalies," *Geophysical Prospecting*, Vol. 53, No. 1, 83–89, 2005.
6. Abdelrahman, E. M. and K. S. Essa, "A new method for depth and shape determinations from magnetic data," *Pure and Applied Geophysics*, Vol. 172, No. 2, 439–460, 2015.
7. Tlas, M. and J. Asfahani, "The simplex algorithm for best-estimate of magnetic parameters related to simple geometric-shaped structures," *Mathematical Geosciences*, Vol. 47, No. 3, 301–316, 2015.
8. Gokturkler, G. and C. Balkaya, "Inversion of self-potential anomalies caused by simple-geometry bodies using global optimization algorithms," *Journal of Geophysics and Engineering*, Vol. 9, No. 5, 498–507, 2012.
9. Biswas, A., "Interpretation of gravity and magnetic anomaly over thin sheet-type structure using very fast simulated annealing global optimization technique," *Modeling Earth Systems and Environment*, Vol. 2, No. 1, 30, 2016.
10. Ekinici, Y. L., "MATLAB-based algorithm to estimate depths of isolated thin dike-like sources using higher-order horizontal derivatives of magnetic anomalies," *Springer Plus*, Vol. 5, No. 1, 1384, 2016.
11. Guo, Z. Y., D. J. Liu, Q. Pan, Y. Y. Zhang, Y. Li, and Z. Wang, "Vertical magnetic field and its analytic signal applicability in oil field underground pipeline detection," *Journal of Geophysics and Engineering*, Vol. 12, No. 3, 340–350, 2015.
12. Feng, S., D. Liu, X. Cheng, H. Fang, and C. Li, "A new segmentation strategy for processing magnetic anomaly detection data of shallow depth ferromagnetic pipeline," *Journal of Applied Geophysics*, Vol. 139, 65–72, 2017.
13. Zhu, H., D. Liu, S. Feng, Q. Pan, and J. Yan, "Magnetic dipole reconstruction geometry modeling for underground ferromagnetic pipe magnetic abnormal detection," *Computer Measurement and Control*, Vol. 25, No. 3, 201, 2017.
14. Biswas, A., M. P. Parija, and S. Kumar, "Global nonlinear optimization for the interpretation of source parameters from total gradient of gravity and magnetic anomalies caused by thin dyke," *Annals of Geophysics*, Vol. 60, No. 2, 0218, 2017.
15. Guo, Z., D. Liu, Q. Pan, and Y. Y. Zhang, "Forward modeling of total magnetic anomaly over a pseudo-2D underground ferromagnetic pipeline," *Journal of Applied Geophysics*, Vol. 113, 14–30, 2015.
16. Wang, F., Y. Song, L. Dong, C. Tao, and X. Lin, "Magnetic anomalies of submarine pipeline based on theoretical calculation and actual measurement," *IEEE Transactions on Magnetics*, Vol. 55, No. 4, 1–10, 2019.
17. Finlay, C. C., et al., "International geomagnetic reference field: The eleventh generation," *Geophysical Journal International*, Vol. 183, No. 3, 1216–1230, 2010.
18. Liu, D. G., et al., "Adaptive cancellation of geomagnetic background noise for magnetic anomaly detection using coherence," *Measurement Science and Technology*, Vol. 26, No. 1, 015008, 2014.
19. Sen, M. K. and P. L. Stoffa, *Global Optimization Methods in Geophysical Inversion*, Cambridge University Press, 2013.
20. Singh, B., "Simultaneous computation of gravity and magnetic anomalies resulting from a 2-D object," *Geophysics*, Vol. 67, No. 3, 801–806, 2002.
21. Eberhart, R. and J. Kennedy, "Particle swarm optimization," *Proceedings of the IEEE International Conference on Neural Networks*, Vol. 4, 1942–1948, 1995.
22. Kennedy, J., "Particle swarm optimization," *Encyclopedia of Machine Learning*, 760–766, 2010.
23. Merchaoui, M., A. Sakly, and M. F. Mimouni, "Particle swarm optimisation with adaptive mutation strategy for photovoltaic solar cell/module parameter extraction," *Energy Conversion and Management*, Vol. 175, 151–163, 2018.
24. Liang, H. and F. Kang, "Adaptive mutation particle swarm algorithm with dynamic nonlinear changed inertia weight," *Optik*, Vol. 127, No. 19, 8036–8042, 2016.
25. Wang, H., W. Wang, and Z. Wu, "Particle swarm optimization with adaptive mutation for multimodal optimization," *Applied Mathematics and Computation*, Vol. 221, 296–305, 2013.

26. Mohurd, *Technical Specification for Urban Underground Pipeline Detection and Survey*, China Building Industry Press, Beijing, 2017.
27. Aleardi, M., A. Tognarelli, and A. Mazzotti, “Characterisation of shallow marine sediments using high-resolution velocity analysis and genetic-algorithm-driven 1D elastic full-waveform inversion,” *Near Surface Geophysics*, Vol. 14, No. 5, 449–460, 2016.